crystals

MDPI

Article

Reduced Sintering Temperatures of Li^+ Conductive $Li_{1.3}Al_{0.3}Ti_{1.7}(PO_4)_3$ Ceramics

Katja Waetzig *, Christian Heubner and Mihails Kusnezoff

Fraunhofer IKTS, Fraunhofer Institute for Ceramic Technologies and Systems IKTS, Winterbergstrasse 28, 01277 Dresden, Germany; christian.heubner@ikts.fraunhofer.de (C.H.); mihails.kusnezoff@ikts.fraunhofer.de (M.K.)

* Correspondence: katja.waetzig@ikts.fraunhofer.de

Received: 6 April 2020; Accepted: 15 May 2020; Published: 20 May 2020

Abstract: All-solid-state batteries (ASSB) are considered promising candidates for future energy storage and advanced electric mobility. When compared to conventional Li-ion batteries, the substitution of Li-ion conductive, flammable liquids by a solid electrolyte and the application of Li-metal anodes substantially increase safety and energy density. The solid electrolyte $Li_{1.3}Al_{0.3}Ti_{1.7}(PO_4)_3$ (LATP) provides high Li-ion conductivity of about 10^{-3} S/cm and is considered a highly promising candidate for both the solid electrolyte-separator and the ionically conductive part of the all-solid state composite cathode, consisting of the cathode material, the solid electrolyte, and an electron conductor. Co-sintering of the composite cathode is a sophisticated challenge, because temperatures above 1000 °C are typically required to achieve the maximum ionic conductivity of LATP but provoke reactions with the cathode material, inhibiting proper electrochemical functioning in the ASSB. In the present study, the application of sintering aids with different melting points and their impact on the sinterability and the conductivity of LATP were investigated by means of optical dilatometry and impedance spectroscopy. The microstructure of the samples was analyzed by SEM. The results indicate that the sintering temperature can be reduced below 800 °C while maintaining high ionic conductivity of up to 3.6×10^{-4} S/cm. These insights can be considered a crucial step forward towards enable LATP-based composite cathodes for future ASSB.

Keywords: Li-ion conductive ceramic; solid electrolyte; Li-ion batteries; all-solid-state batteries; LATP

1. Introduction

All-solid-state batteries (ASSB) are considered as promising candidates for future energy storage and advanced electric mobility. When compared to conventional Li-ion batteries, the substitution of Li-ion conductive, flammable liquids by a solid electrolyte and the application of Li-metal anodes substantially increase safety and energy density [1]. When compared to common Li-ion batteries (LIB) currently used in mobile electronic devices and electric vehicles, the liquid electrolyte is substituted by a solid Li-ion conductor in the ASSB [2]. This includes a solid electrolyte-separator and the ionically conductive part of the all-solid state composite cathode, consisting of a cathode material, the solid electrolyte, and an electron conductor. Besides advantages regarding energy density, the substitution of the flammable liquid electrolyte will improve the safety significantly. Three types of materials have proven to be promising for this approach: polymers, sulfides, and oxides [3]. The polymers are easy to handle under dry air and production is scalable, but the Li-ion conductivity at room temperature is limited to the range of 10^{-6}–10^{-5} S/cm and can be increased by heating at 60 °C to $>10^{-4}$ S/cm [4]. In contrast, sulfides exhibit high Li-ion conductivity of $\sim 10^{-3}$ S/cm at room temperature, but require extreme pressures [5]. Furthermore, sulfides are very sensitive to moisture, which necessitates handling under inert conditions. Oxides are not affected by these restrictions and

can be fabricated in large batches under normal conditions [6]. Moreover, oxides such as garnet-type (Li-La-Zr oxide) or phosphates (Li-Al-Ti phosphate) provide high Li-ion conductivity in the range of 10^{-4}–10^{-3} S/cm after sufficient densification via a sintering step at high temperature [7,8]. However, the high sintering temperatures lead to two major challenges for cathodes with solid electrolytes: (i) Li loss by vaporization of Li_2O [9] and (ii) irreversible reactions between the solid electrolytes and the active material (e.g., Ni-rich NCM622 $LiNi_{0.6}Co_{0.2}Mn_{0.2}O_2$) during co-sintering of the composite cathode, forming other non-conductive phases [10–12]. In both cases, the material is irreversibly damaged and leads to poor electrochemical performance. Although, the sintering temperature of the phosphates (1000–1100 °C) is lower than for the garnets (1200–1300 °C), the reactivity with active materials is still too high to avoid significant reactions during co-sintering with cathode materials [13]. Thus, to enable these promising oxides as solid electrolytes in ASSB, a key objective is the reduction of the sintering temperature while preserving excellent conductivity.

For the $Li_{1.3}Al_{0.3}Ti_{1.7}(PO_4)_3$ stoichiometry, the Li-ion conductivity of single crystals is approximately 5×10^{-3} S/cm [14]. The effective Li-ion conductivity of polycrystalline $Li_{1.3}Al_{0.3}Ti_{1.7}(PO_4)_3$ (LATP) is decreased by microstructural defects, such as grain boundaries, pores, and cracks, e.g., $\leq 1 \times 10^{-3}$ S/cm (25 °C) after sintering at high pressure [15]. Sintering LATP ceramics under application-oriented processing conditions (pressureless, air atmosphere) yields even higher porosity, resulting in further reduction of the Li-ion conductivity (2–4 $\times 10^{-4}$ S/cm), which is approximately one order of magnitude below the bulk conductivity of single crystals [16]. To lower the sintering temperature while achieving high ionic conductivity, several researchers proposed the application of sintering aids. Rosero-Navarro et al. optimized the Al_2O_3 and Li_3BO_3 content as sintering additives for garnet type $Li_{7-x}La_{2.95}Ca_{0.05}ZrTaO_{12}$ and found increased ionic conductivity and densification at low sintering temperatures [17]. For the NASICON type, Aono et al. [18] reported reduced sintering temperatures of $LiTi_2(PO_4)_3$ (LTP) by using sintering aids. Particularly, Li_3BO_3 (Li_2CO_3 + H_3BO_3) and Li_3PO_4 salts are found to decrease the sintering temperature from 1260 to 800 °C, while simultaneously reducing cracks, producing glass filled pores, and improving the conductivity by two orders of magnitude (2×10^{-6} S/cm to 3×10^{-4} S/cm). The addition of $LiNO_3$ salt decreases the sintering temperature of LTP by melting and solidification and improves the conductivity to approximately 10^{-5} S/cm [19]. Kwatek et al. [20,21] showed that the addition of Li_3BO_3 or $Li_{2.9}B_{0.9}S_{0.1}O_{3.1}$ glass (Li_2CO_3 + H_3BO_3 + Li_2SO_4) to $LiTi_2(PO_4)_3$-based composites significantly increases the total ionic conductivity by almost four orders of magnitude to a maximum of 1.8×10^{-4} S/cm when compared to pure $LiTi_2(PO_4)_3$ ceramics. Furthermore, the addition of $LiTiOPO_4$ lowers the sintering temperatures and increases densification of the studied LATP and LTP, which leads to enhanced ionic conductivity of the composite [22]. Indeed, even the application of insulating sintering aids improves the ionic conductivity of NASICON-type materials, pointing out the huge impact of the microstructure on the effective conductivity [23]. Novel sintering technologies for densification with decreased temperatures, such as cold sintering, have been recently reported and describe the compaction of $Li_{1.3}Al_{0.3}Ti_{1.7}(PO_4)_3$ (LATP) at T = 120 °C with post-annealing (650 °C) [24]. LATP samples prepared by this way show a maximum room temperature ionic conductivity and relative density of 8×10^{-5} S/cm and 93%, respectively.

In the present study, we systematically investigated the reduction of the sintering temperature of solid electrolytes for ASSB with NASICON structure by the application of sintering aids, using the exemplary composition of $Li_{1.3}Al_{0.3}Ti_{1.7}(PO_4)_3$ (LATP). The influence of sintering aids with different melting points was comparatively investigated regarding the sinterability of LATP. The sintering process and the resulting Li-ion conductivity were analyzed by optical dilatometry and impedance spectroscopy, respectively. The sintering behavior and achieved properties of the samples were correlated with their microstructure, analyzed by scanning electron microscopy (SEM). The results are discussed regarding the fabrication of LATP based composite cathodes for future ASSB.

2. Materials and Methods

Figure 1 shows the experimental workflow of preparing Li^+ conductive LATP ceramics. $Li_{1.3}Al_{0.3}Ti_{1.7}(PO_4)_3$ (LATP) powder with high phase purity was prepared by sol–gel synthesis as reported previously [15]. After milling, the average particle size was determined to be d_{50} = 0.76 µm with laser diffraction in a particle size range between 20 nm and 2000 µm (Mastersizer 2000, Malvern Instruments Ltd., Malvern, UK). The powder was mixed with 15 mol% sintering aid by wet-milling in ethanol. Table 1 lists the sintering aids used together with their respective melting points. Intension for addition of sintering aids with melting points below the sintering temperature of LATP was to induce the liquid phase sintering and in this way reduce the sintering temperature. The milling step was performed for two hours in a planetary micro mill (Pulverisette 7, Fritsch, Germany) with milling balls and cups made of zirconia. The suspension was dried in air for 12 h. After grinding in a mortar, the powder was pressed into cylindrical discs of 8 mm in diameter and 2 mm in height. The discs were sintered by application of a heating ramp (3 K/min) followed by 1 h dwell time. The final temperature was varied between 700 and 1100 °C. After sintering, the density was calculated by the geometrical data and the mass of each specimen. The density value was determined as an average of three samples with a standard deviation of ≤0.08 g/cm^3. The relative densities were determined using the experimentally obtained densities and the theoretical density of bulk LATP (2.94 g/cm^3).

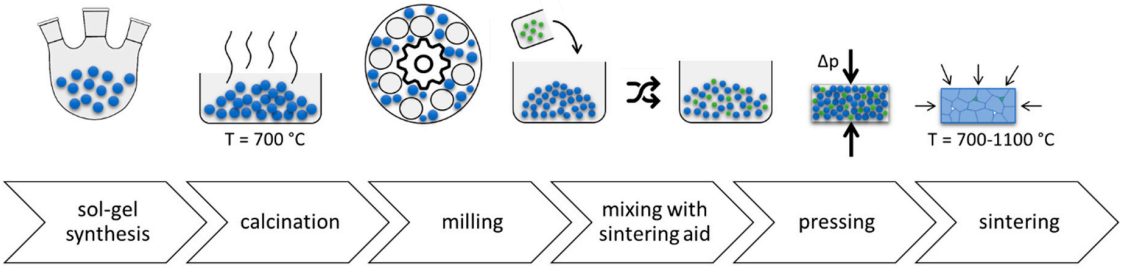

Figure 1. Experimental workflow of preparing Li conductive $Li_{1.3}Al_{0.3}Ti_{1.7}(PO_4)_3$ (LATP) ceramics.

Table 1. Sintering additives with melting point (taken from the data sheet of the chemicals producer and the phase diagram Li-B-O [25]).

Sintering Aid	Melting Point °C
LiOH	462
LiCl	605
Li_3BO_3 (mixture of Li_2CO_3 and $LiBO_2$)	665
Li_2CO_3	723
Li_3PO_4	837
$LiBO_2$	849

For analyzing the shrinkage behavior by optical dilatometry, the powder mixtures were pressed into cylindrical shapes with 2 mm diameter and 2 mm height and placed in the EM301 heating microscope (Hesse Instruments, Osterode, Germany). The shrinkage behavior was measured during application of a heating ramp (5 K/min) and a final temperature of 1200 °C. The linear shrinkage was determined by EMI III heating microscope software (Hesse Instruments, Osterode, Germany). Based on these data, the shrinkage rate was calculated as first derivation.

The ionic conductivity of the LATP ceramics was determined by impedance spectroscopy. For this purpose, the samples were sputtered with gold as ion-blocking electrodes. The impedance spectra were measured at room temperature using a potentiostat (VMP3, Biologic) in a frequency range from 10^6 to 10^{-2} Hz and a p-p amplitude of 20 mV. The impedance data were fitted to an appropriate electrical equivalent circuit. The fit results are used to calculate the ionic conductivity, taking into account the geometry of the samples. The calculated values were not corrected for porosity.

3. Results and Discussions

Figure 2 compares the shrinkage behaviors of pure LATP and the different mixtures of LATP and sintering aids. The sintering temperature was significantly reduced and the maximum shrinkage rate was enhanced for all mixtures of LATP with sintering aids when compared to pure LATP. The lowest sintering temperature of about 730 °C was reached with the mixture of Li_2CO_3 and $LiBO_2$ (forming Li_3BO_3 with eutectic melting point of T = 665 °C). The addition of Li_2CO_3 as well as Li_3PO_4 resulted in slightly higher sintering temperatures of approximately 760 °C (cf. Figure 2a). $LiBO_2$ and LiOH reduced the sintering temperature of LATP to approximately 800 °C (cf. Figure 2b). Mixtures with LiCl salt as additive showed the smallest impact on both the sintering temperature (840 °C) and the shrinkage rate. Interestingly, the influence of the different additives on the sintering temperature and the maximum shrinkage rate did not correlate with their specific melting points, as depicted in Figure 3 by plotting the temperature of the maximum shrinkage rate against the melting point of the sintering aids.

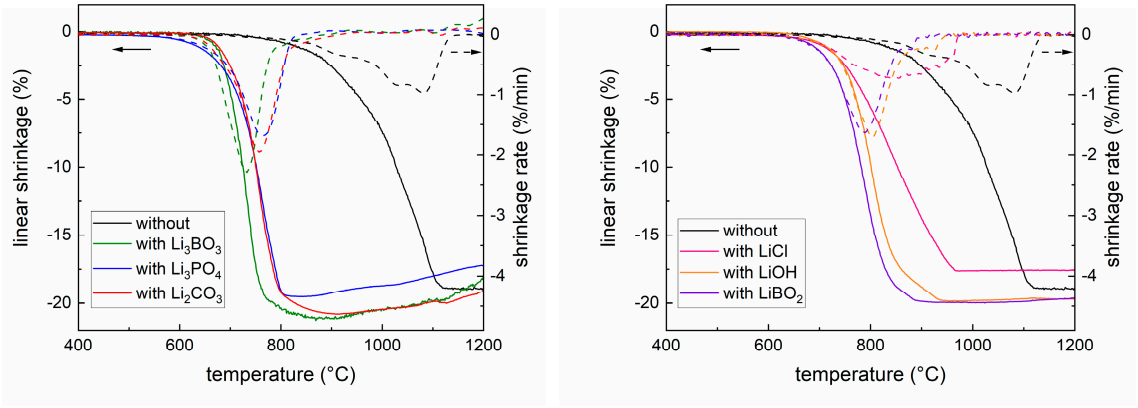

Figure 2. Linear shrinkage (solid line) and shrinkage rate (dashed line) of sol–gel synthesized LATP powder after milling with/without sintering aids. (**a**) sintering aids: Li_3BO_3, Li_3PO_4, and Li_2CO_3, and (**b**) LiCl, LiOH, and $LiBO_2$.

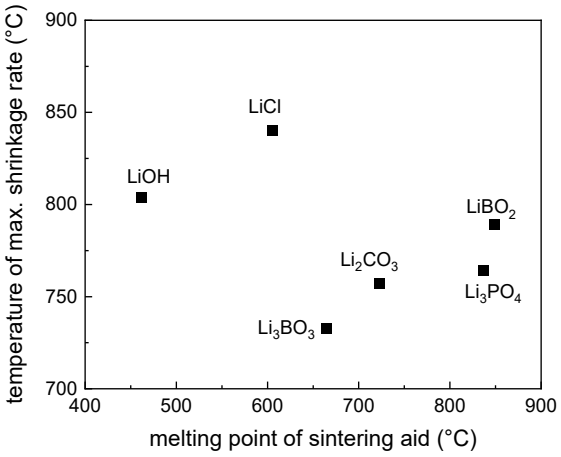

Figure 3. Melting temperature of the sintering aids as a function of the maximum temperature of the shrinkage rate of LATP powder mixed with 15 mol% sintering aid.

The investigated sintering additives considerably improved the shrinkage behavior of LATP and reduced the sintering temperature by more than 200 K. We explain these phenomena by the solution and precipitation process of the Li salts on the surface of the LATP particles during heating, so that local melting and disorder accelerates the surface diffusion as a driving force for sintering.

However, it has to be considered that the sintering behavior and associated densification are also affected by the homogeneity of the mixture, the mobility of the ions, and the wetting behavior. Most probably, these properties vary with the type of sintering aid, resulting in the different behaviors observed in Figure 2.

Mixtures of LATP with Li_3BO_3, Li_3PO_4, and Li_2CO_3, respectively, were selected for further investigation because they showed the most promising sintering behavior. The powder mixtures were pressed into discs and sintered with short dwell times followed by comprehensive materials characterization. Figure 4 depicts the relative density of sintered LATP ceramics with and without sintering aids. As expected from the analysis of the shrinkage behavior, the densification of the mixtures with sintering aids occurred between 700 and 800 °C (cf. Figure 4). In contrast, densifying the pure LATP required temperatures higher than 1000 °C. It has to be noted that for sintering at T = 1100 °C, cracking of the samples was observed. This effect is known for sintering of LATP. It is related to an anisotropic grain growth at high temperature and associated tensions in the microstructure, which result in cracking [9,26]. In this case, a reliable determination of the density was not possible.

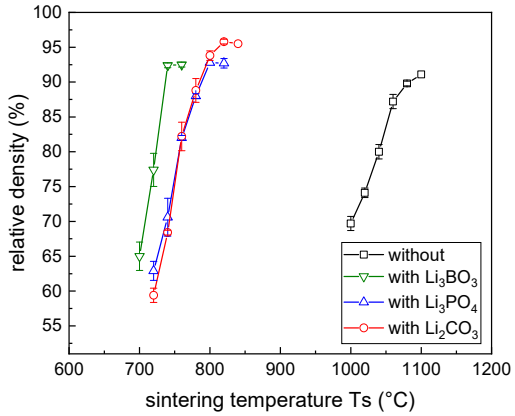

Figure 4. Relative density of sintered samples with/without 15 mol% sintering aids mixed with LATP as a function of sintering temperature Ts (dwell time at Ts is 1 h).

Figure 5 shows typical impedance spectra in the Nyquist plot obtained from the LATP samples sputtered with ion-blocking gold electrodes for different sintering temperatures (Figure 5a) and sintering aids (Figure 5b). All spectra show a semi-circle at high frequencies and a straight line at medium to low frequency ranges. The latter is known to be related to the capacitive charging of the interface between the sample and the ion-blocking electrode. The semi-circle is attributed to a relaxation process of charge carriers in the LATP sample. Figure 5 indicates that both the sintering temperature and the type of sintering aid affect the impedance of the samples.

Typically, the impedance spectra of ionic conducting ceramics exhibit two distinct features attributable to bulk and grain boundary impedance (c.f. Figure 6a) with typical capacitances of $C_b \sim 10^{-12}$ and $C_{gb} \sim 10^{-11}$–10^{-8} F/cm, respectively [27]. In this case, the impedance was successfully fitted by the equivalent circuit shown in Figure 6a. The bulk phase had a very low time constant ($\tau_b = R_b C_b$) and the relaxation frequency of the corresponding semi-circle was located in the MHz range. For this reason, this semi-circle was not visible in our impedance spectra. Nevertheless, the impedance data fit the semi-circle related to the grain boundary very well ($\chi^2/|Z| < 10^{-3}$). Consequently, to fit the whole impedance spectra, a simplified equivalent circuit can be used ($R_b + R_{gb}|Q_{gb} + Q_{int}$), with Q being a constant phase element. With this procedure, the specific capacitance of the bulk contribution could not be determined, but the resistance associated with bulk conductivity was estimated with sufficient accuracy. Figure 6b shows the total ionic conductivity of the LATP samples and the individual contributions of the bulk material and the grain boundaries calculated from the obtained R_b and R_{gb} values and plotted against the sintering temperature. The bulk conductivity increased slightly with increasing sintering temperature or relative density and was almost constant and close to the values

reported for single crystals for samples with relative density > 90% exhibit similar grain boundary capacitance as for high temperature sintered pure LATP (see Figure 7b), which supports the accuracy of the impedance analysis. The conductivity of the grain boundaries, which limits the total ionic conductivity, increased strongly with higher sintering temperature for all samples containing sintering aids. The porosity of the samples decreased with increasing sintering temperature and had a positive impact on R_{gb}. Comparing the results to those obtained on samples with relative density >90%, the highest conductivity of the grain boundaries was obtained with Li_2CO_3 as the sintering additive.

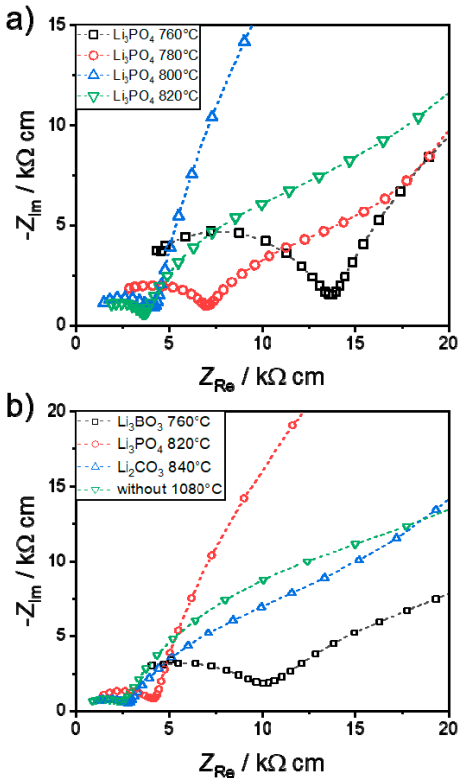

Figure 5. Room temperature impedance spectra obtained from the LATP samples sputtered with gold as ion blocking electrodes for (**a**) different sintering temperature using the example of Li_3PO_4 as the sintering aid and (**b**) different sintering aids for the respective highest sintering temperature.

To achieve insight regarding the impact of sintering aids and temperature on the properties of the LATP samples, we analyzed the specific capacitance of the grain boundaries determined by fitting the impedance data. Figure 7a shows that specific capacitance of the grain boundaries clearly increased with the sintering temperature for samples prepared with sintering aids. Generally, the specific capacitance of the grain boundaries was strongly affected by microstructural properties, such as pores, grain sizes, the thickness of the intergranular regions, and the homogeneity of the grain boundary phase. Moreover, the relative permittivity of the grain boundary phase was affected by the composition, which might vary for the different sintering aids and temperatures. In the case of completely dense sintered materials, the capacitance was expected to increase for a narrowing of the intergranular regions [27]. Although this was not fully achieved in the present case, it was found that samples with Li_2CO_3 (relative density > 90%) exhibited similar grain boundary capacitance as that of high temperature sintered pure LATP (see Figure 7b), which indicates that similar sintering quality can be achieved at temperatures as low as 800 °C by applying sintering aids. The impact of the different sintering aids was comparably strong for Li_2CO_3, Li_3PO_4, and Li_3BO_3, nevertheless, the Li_2CO_3 seemed to have the most positive effect on the densification and the conductivity of the grain boundaries and bulk.

Without sintering additives, the Li-ion conductivity of the LATP reached a maximum value of 3.8×10^{-4} S/cm after sintering at a temperature of 1080 °C (Figure 6b, Table 1). Comparable values

were obtained for LATP with Li_3PO_4 and Li_2CO_3 sintered at much lower temperatures. For example, in the case of Li_2CO_3, a conductivity of 3.6×10^{-4} S/cm was achieved for sintering at T = 840 °C. By comparison, the conductivities of samples prepared with Li_3PO_4 as the sintering aid were slightly lower. The differences found for the different sintering aids correlated with differences observed in samples' microstructures (Figure 8). In the case of LATP with Li_2CO_3 as the sintering aid, the open porosity was progressively reduced with increased sintering temperature, whereby the sintering additive seemed to be located in the triple point between the grains or was dissolved in the LATP lattice. At a density of 96%, the microstructure was densified homogeneously with only slight amounts of residual pores between and inside the grains. In this final sintering stage, the Li_2CO_3 seemed to be decomposed or dissolved in the structure and was not detectable by SEM-EDX. In the case of Li_3PO_4 as the sintering aid, the microstructure with density of ~93% also showed residual porosity but a higher amount of the additive in the triple points between the grains or glassy filled pores (Figure 9a). This local distribution of the sintering aid between the grains might cause the slightly decreased conductivity when compared to that of Li_2CO_3. Cross-sectional preparation of the LATP samples must be conducted under inert atmosphere or vacuum to avoid unwanted reactions, e.g., with moisture. Unfortunately, cross-sectional preparation by ion beam polishing does not etch the grain boundaries to visualize the microstructure more clearly (Figure 9). Therefore, the exact position of the sintering aids (grain boundaries or triple points) could not be elucidated in more detail in the current stage of development, but is the subject matter of ongoing work.

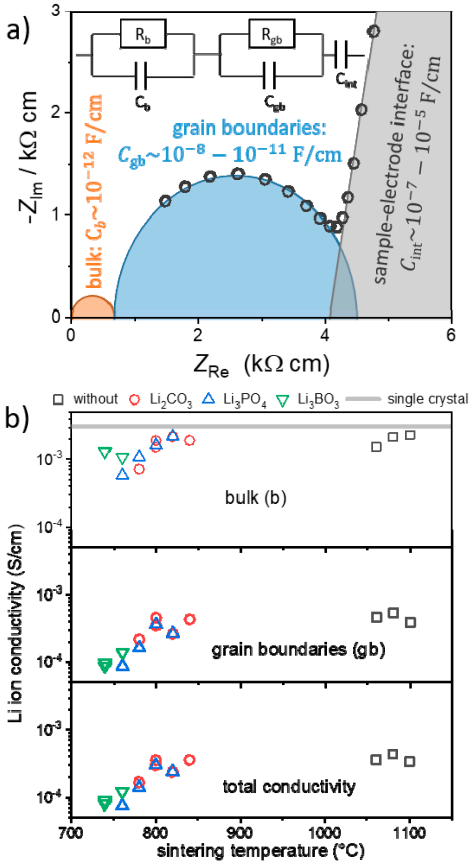

Figure 6. (**a**) Nyquist representation of a typical impedance spectrum obtained from an LATP sample sintered at 820 °C with 15 mol% Li_3PO_4 as the sintering aid together with an interpretative approach and the corresponding electrical equivalent circuit. (**b**) Total ionic conductivity of the LATP samples with different sintering aids and the individual contributions of the bulk material and the grain boundaries plotted against the sintering temperature.

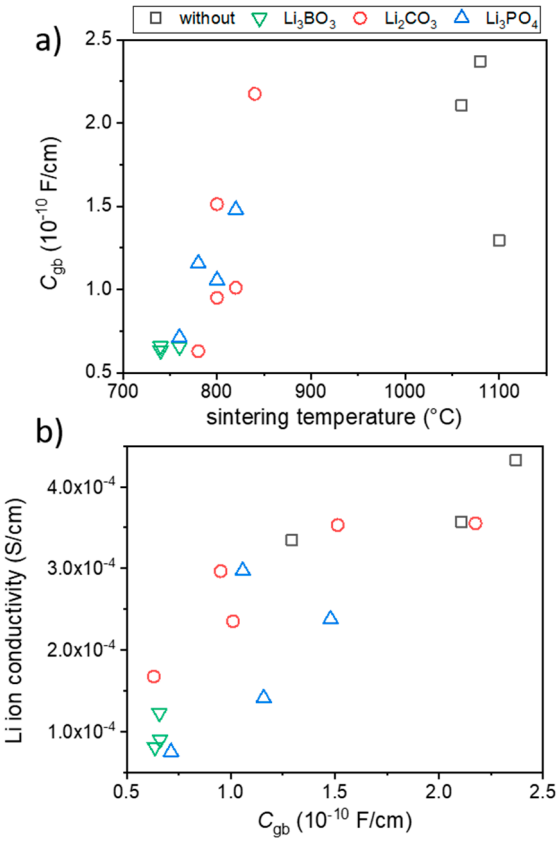

Figure 7. (**a**) Capacitance of the grain boundaries as a function of the sintering temperature and (**b**) Li-ion conductivity plotted against the capacitance of the grain boundaries.

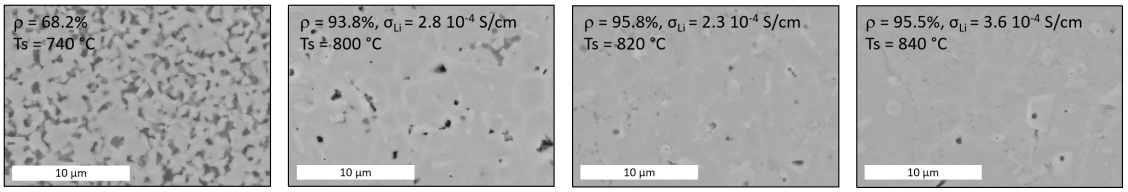

Figure 8. Microstructure of sintered LATP with Li_2CO_3 as the sintering aid at different stages of densification.

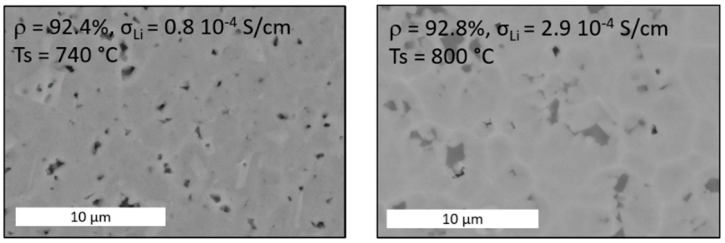

Figure 9. Microstructure of sintered LATP with (**a**) Li_3PO_4 or (**b**) Li_3BO_3 at a comparable stage of densification.

In Figure 10, the phase composition of the LATP ceramics without sintering aids and with Li_3BO_3, Li_3PO_4, and Li_2CO_3 addition analyzed by XRD is shown. The sample without sintering aids had a density of 89.8% and consisted of LATP and a small amount of rutile (TiO_2). Whereas, the diffraction pattern of samples with sintering aids showed LATP as the main phase with small amounts of rutile,

Li(Ti,Al)OPO_4, and $Li_2P_4O_7$ (only for Li_3PO_4 addition). In all cases, the sintering additives were not detected in the final sintered material, which suggests a solution and phase separation process during heat treatment. The solubility of the sintering additives seems not to be high enough, so that the Li(Al,Ti)OPO_4 phase as the second crystalline phase in the Li_2O-TiO_2-P_2O_5 system with higher Li_2O content was formed. The amount of the secondary phase seems to be low and cannot explain the difference of one order of magnitude in Li-ion conductivity between ceramics sintered with Li_3BO_3 and those with Li_2CO_3. The most reasonable explanation for this difference is the unfavorable composition of the grain boundary phase in the case of Li_3BO_3, whose composition however cannot be determined by XRD.

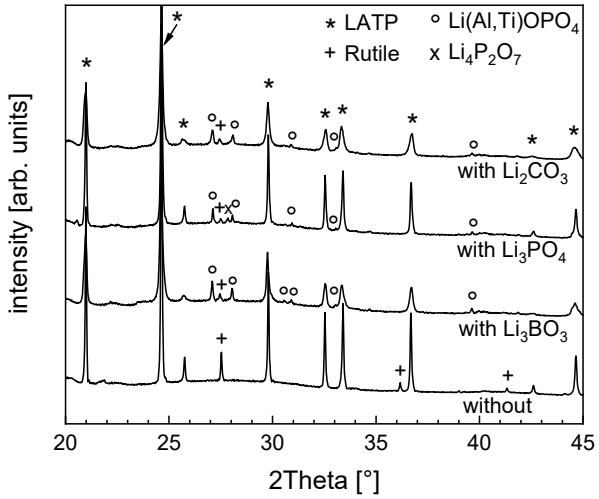

Figure 10. X-ray diffraction pattern of sintered LATP without additives (T_S = 1080 °C, ρ = 89.9%), with Li_3BO_3 (T_S = 740 °C, ρ = 92.4%), with Li_3PO_4 (T_S = 820 °C, ρ = 92.7%), and Li_2CO_3 (T_S = 820 °C, ρ = 95.8%) referenced with PDF 01-072-6140 ($LiTi_2(PO_4)_3$ for LATP), PDF 01-089-0554 (Rutile), PDF 00-044-0083 ($LiTiOPO_4$ for Li(Al,Ti)OPO_4), and PDF 01-078-6750 ($Li_4P_2O_7$).

Aono et al. [18] reported decreased sintering temperatures and improved conductivity for $LiTi_2(PO_4)_3$ with Li_3PO_4 and Li_3BO_3 as sintering aids. The present systematic study revealed that in the case of LATP, the lowest sintering temperature was achieved by adding Li_3BO_3. However, the Li-ion conductivity (9.8×10^{-5} S/cm) was reduced in comparison to the other sintering aids investigated.

In this study, the highest total Li-ion conductivity of 3.8×10^{-4} S/cm for $Li_{1.3}Al_{0.3}Ti_{1.7}(PO_4)_3$ sintered with Li_2CO_3 was about one magnitude lower compared to 5×10^{-3} S/cm of single crystals [14] with the same composition. The bulk conductivity of crystalline phase obtained from EIS (2×10^{-3} S/cm, see Figure 6b) showed values close to those of single crystals. The microstructural and phase analyses suggest that for sintered samples with high density, the amount, composition, thickness, and distribution of grain boundary phase in the microstructure (i.e., at triple points or along the grains); secondary phases (rutile and Li(Ti,Al)OPO_4 phases); and residual porosity are the main factors influencing the ionic conductivity.

4. Conclusions

$Li_{1.3}Al_{0.3}Ti_{1.7}(PO_4)_3$ (LATP) solid electrolyte sintered at 1080 °C provided an excellent Li-ion conductivity of 3.8×10^{-4} S/cm, which appears promising for the application in an all-solid-state composite cathode consisting of an active storage material, the solid electrolyte, and an electron conductor. However, co-sintering of these components required much lower temperatures to avoid chemical reactions that led to poor electrochemical performance. The sintering activity of $Li_{1.3}Al_{0.3}Ti_{1.7}(PO_4)_3$ (LATP) at low temperature can be improved significantly by adding sintering aids.

The sintering temperature, associated with the maximum shrinkage rate, ranged in the following order for adding 15 mol% of the respective sintering aids:

Li_3BO_3 (730 °C) < Li_2CO_3 = Li_3PO_4 (760 °C) < $LiBO_2$ (790 °C) < LiOH (810 °C) < LiCl (840 °C).

Interestingly, the respective impact on the shrinkage behavior did not correlate with the melting point of the aids. Li_3BO_3 had the most significant impact on the sintering temperature. The highest Li-ion conductivity of 3.6×10^{-4} S/cm was achieved by adding Li_2CO_3 as the sintering aid. In this case, the densification of the microstructure was improved even at temperatures as low as 840 °C, which was caused by the lowest grain boundary resistance observed in well-densified samples. The reason for low grain boundary resistance is the decomposition and evaporation or dissolution of the additive into the LATP structure in the final sintering stage. This leads to similar grain boundary resistance as that in material sintered without sintering aids. These novel insights concerning the reduction of the sintering temperature of LATP-based solid electrolytes are a first but important step towards co-sintered composite cathodes for all-solid-state Li-ion batteries.

Author Contributions: Conceptualization, investigation, and evaluation of the material preparation and characterization, writing and editing the draft, submission and revision of the manuscript: K.W. Investigation and evaluation of the impedance characterization, writing and editing the draft: C.H. Writing and editing the manuscript, interpretation of observed phenomena, supervision: M.K. All authors have read and agreed to the published version of the manuscript.

Funding: This research was funded by the German Federal Ministry of Education and Research (Germany) grant number 03XP0173D.

Acknowledgments: The authors would like to thank K. Jungnickel, I. Eichler, and E. Pfannmöller for sol–gel synthesis, preparation of the mixtures, pressing and sintering, and measurement of the density and the shrinkage behavior; M. Striegler and colleagues for ceramographical preparation and SEM images; and A. Nickol for impedance measurements. The authors acknowledge financial support by the German Federal Ministry of Education and Research (Germany) in the cluster of competence for solid-state batteries "FestBatt" (03XP0173D).

Conflicts of Interest: The authors declare that they have no known competing financial interests or personal relationships that could appear to have influenced the work reported in this paper.

References

1. Janek, J.; Zeier, W.G. A solid future for battery development. *Nat. Energy* **2016**, *1*, 16141. [CrossRef]
2. Manthiram, A.; Yu, X.; Wang, S. Lithium battery chemistries enabled by solid-state electrolytes. *Nat. Rev. Mater.* **2017**, *2*, 16103. [CrossRef]
3. Zhao, Q.; Stalin, S.; Zhao, C.-Z.; Archer, L.A. Designing solid-state electrolytes for safe, energy-dense batteries. *Nat. Rev. Mater.* **2020**. [CrossRef]
4. Mindemark, J.; Lacey, M.J.; Bowden, T.; Brandell, D. Beyond PEO–Alternative host materials for Li^+-conducting solid polymer electrolytes. *Prog. Polym. Sci.* **2018**, 114–143. [CrossRef]
5. Koerver, R.; Aygün, I.; Leichtweiß, T.; Dietrich, C.; Thang, W.; Binder, J.O.; Hartmann, P.; Zeier, W.G.; Janek, J. Capacity Fade in Solid-State Batteries: Interphase Formation and Chemomechanical Processes in Nickel-Rich Layered Oxide Cathodes and Lithium Thiophosphate Solid Electrolytes. *Chem. Mater.* **2017**, *29*, 5574–5582. [CrossRef]
6. Ma, Q.; Xu, Q.; Tsai, C.-L.; Tietz, F.; Guillon, O. A Novel Sol-Gel Method for Large-Scale Production of Nanopowders: Preparation of $Li_{1.5}Al_{0.5}Ti_{1.5}(PO_4)_3$ as an Example. *J. Am. Ceram. Soc.* **2016**, *99*, 410–414. [CrossRef]
7. Bucharsky, E.C.; Schell, K.G.; Hintennach, A.; Hoffmann, M.J. Preparation and characterization of sol-gel derived high lithium ion conductive NZP-type ceramics $Li_{1+x}Al_xTi_{2-x}(PO_4)_3$. *Solid State Ion.* **2015**, *274*, 77–82. [CrossRef]
8. Inada, R.; Yasuda, S.; Hosokawa, H.; Saito, M.; Tojo, T.; Sakurai, Y. Formation and Stability of Interface between Garnet-Type Ta-doped $Li_7La_3Zr_2O_{12}$ Solid Electrolyte and Lithium Metal Electrode. *Batteries* **2018**, *4*, 26. [CrossRef]
9. Waetzig, K.; Rost, A.; Langklotz, U.; Matthey, B.; Schilm, J. An explanation of the microcrack formation in $Li_{1.3}Al_{0.3}Ti_{1.7}(PO_4)_3$ ceramics. *J. Eur. Ceram. Soc.* **2016**, *36*, 1995–2001. [CrossRef]
10. Zhu, Y.; He, X.; Mo, Y. First priniciples study on electrochemical and chemical stability of solid electrolyte-electrode interfaces in all-solid-state Li-ion batteries. *J. Mater. Chem. A* **2016**, *4*, 3253. [CrossRef]

11. Tsai, C.-L.; Ma, Q.; Dellen, C.; Lobe, S.; Vondahlen, F.; Windmüller, A.; Grüner, D.; Zheng, H.; Uhlenbruck, S.; Finsterbusch, M.; et al. A garnet structure-based all-solid-state Li battery without interface modification: Resolving incompatibility issues on positive electrodes. *Sustain. Energy Fuels* **2019**, *3*, 280. [CrossRef]
12. Xiao, Y.; Wang, Y.; Bo, S.-H.; Kim, J.C.; Miara, L.J.; Ceder, G. Understanding interface stability in solid-state batteries. *Nat. Rev. Mater.* **2020**, *5*, 105–126. [CrossRef]
13. Miara, L.; Windmüller, A.; Tsai, C.-L.; Richards, W.D.; Ma, Q.; Uhlenbruck, S.; Guillon, O.; Ceder, G. About the Compatibility between High Voltage Spinel Cathode Materials and Solid Oxide Electrolytes as a Function of Temperature. *Appl. Mater. Interfaces* **2016**, *8*, 26842–26850. [CrossRef] [PubMed]
14. Rettenwander, D.; Welzl, A.; Pristat, S.; Tietz, F.; Taibl, S.; Redhammer, G.J.; Fleig, J. A microcontact impedance study on NASICON type $Li_{1+x}Al_xTi_{2-x}(PO_4)_3$ ($0 \leq x \leq 0.5$) single crystals. *J. Mater. Chem. A* **2016**, *4*, 1506. [CrossRef]
15. Waetzig, K.; Rost, A.; Heubner, C.; Coeler, M.; Nikolowski, K.; Wolter, M.; Schilm, J. Synthesis and sintering of $Li_{1.3}Al_{0.3}Ti_{1.7}(PO_4)_3$ (LATP) electrolyte for ceramics with improved Li^+ conductivity. *J. Alloy. Compd.* **2020**, *818*, 153237. [CrossRef]
16. Duluard, S.; Paillassa, A.; Lenormand, P.; Taberna, P.-L.; Simon, P.; Rozier, P.; Ansart, F. Dense on porous solid LATP electrolyte system: Preparation and conductivity measurement. *J. Am. Ceram. Soc.* **2017**, *100*, 141–149. [CrossRef]
17. Rosero-Navarro, N.C.; Miura, A.; Higuchi, M.; Tadanaga, K. Optimization of Al_2O_3 and Li_3BO_3 Content as Sintering Additives of $Li_{7-x}La_{2.95}Ca_{0.05}ZrTaO_{12}$ at Low Temperature. *J. Electr. Mater.* **2017**, *46*, 497–501. [CrossRef]
18. Aono, H.; Sugimoto, E.; Sadaoka, Y.; Imanaka, N.; Adachi, G.-Y. Electrical property and sinterability of $LiTi_2(PO_4)_3$ mixed with lithium salt (Li_3PO_4 or Li_3BO_3). *Solid State Ion.* **1991**, *47*, 257–264. [CrossRef]
19. Kobayashi, Y.; Tabuchi, M.; Nakamura, O. Ionic conductivity enhancement in $LiTi_2(PO_4)_3$-based composite electrolyte by the addition of lithium nitrate. *J. Power Sources* **1997**, *68*, 407–411. [CrossRef]
20. Kwatek, K.; Nowiński, J.L. Solid lithium ion conducting composites based on $LiTi_2(PO_4)_3$ and $Li_{2.9}B_{0.9}S_{0.1}O_{3.1}$ glass. *Solid State Ion.* **2018**, *322*, 93–99. [CrossRef]
21. Kwatek, K.; Świniarski, M.; Nowiński, J.L. The Li^+ conducting composite based on $LiTi_2(PO_4)_3$ and Li_3BO_3 glass. *J. Solid State Chem.* **2018**, *265*, 381–386. [CrossRef]
22. Hupfer, T.; Bucharsky, E.C.; Schell, K.G.; Hoffmann, M.J. Influence of the secondary phase $LiTiOPO_4$ on the properties of $Li_{1+x}Al_xTi_{2-x}(PO_4)_3$ (x = 0; 0.3). *Solid State Ion.* **2017**, *302*, 49–53. [CrossRef]
23. Kyono, N.; Bai, F.; Nemori, H.; Minami, H.; Mori, D.; Takeda, Y.; Yamamoto, O.; Imanishi, N. Lithium-ion conducting solid electrolytes of $Li_{1.4}Al_{0.4}Ge_{0.2}Ti_{1.4}(PO_4)_3$ and MOx (M=Al, Ti, and Zr) composites. *Solid State Ion.* **2018**, *324*, 114–127. [CrossRef]
24. Liu, Y.; Liu, J.; Sun, Q.; Wang, D.; Adair, K.R.; Liang, J.; Zhang, C.; Zhang, L.; Lu, S.; Huang, H.; et al. Insight into the Microstructure and Ionic Conductivity of Cold Sintered NASICON Solid Electrolyte for Solid-State Batteries. *ACS Appl. Mater. Interfaces* **2019**, *11*, 27890–27896. [CrossRef] [PubMed]
25. Maraine-Giroux, C.; Bouaziz, R.; Perez, G. The devitrification of lithium metaborate: Polymorphism and glass formation. *Rev. Chim. Miner.* **1972**, *9*, 779–787.
26. Jackman, S.D.; Cutler, R.A. Effect of microcracking on ionic conductivity in LATP. *J. Power Sources* **2012**, *218*, 65–72. [CrossRef]
27. Irvine, J.T.S.; Sinclair, D.C.; West, A.R. Electroceramics: Characterization by Impedance Spectroscopy. *Adv. Mater.* **1990**, *2*, 132–138. [CrossRef]